Heat-Induced Self-Assembling of Thermosensitive Block Copolymer. 1. Small-Angle Neutron Scattering Study

Satoshi Okabe,[†] Shinji Sugihara,[‡] Sadahito Aoshima,[‡] and Mitsuhiro Shibayama*[,†]

Neutron Scattering Laboratory, Institute for Solid State Physics, The University of Tokyo, Tokai, Ibaraki, 319-1106, Japan; and Department of Macromolecular Science, Graduate School of Science, Osaka University, Toyonaka, Osaka 560-0043, Japan

Received March 25, 2002; Revised Manuscript Received June 24, 2002

ABSTRACT: The sharp and thermoreversible morphological transitions of poly(2-ethoxyethyl vinyl ether-*b*-2-hydroxyethyl vinyl ether) (poly(EOVE-*b*-HOVE)) in aqueous solutions have been investigated by means of small-angle neutron scattering. The poly(EOVE-*b*-HOVE), synthesized by living cationic polymerization, had the number-average degree of polymerizations of the constituent blocks of 200 and 400, respectively, and a polydispersity index of 1.07. The poly(EOVE-*b*-HOVE) underwent a disorder−order transition around 17−21 °C, depending on the polymer concentration. This is a micellization with a poly(EOVE) core of ca. 20 nm in radius and a poly(HOVE) corona. When the polymer concentration was high enough, e.g., 17 wt %, a macrolattice formation with body-centered cubic symmetry was also observed. This transition took place in a narrow temperature window of less than a degree centigrade. The origin of this sharp transition was found to be a dissociation of hydrophobically associated structure, such as an iceberg structure. The enthalpy involved in this dissociation was estimated to be 2.05 kcal/mol of an EOVE monomeric unit, which is about twice as large as that of a well-known thermosensitive polymeric system, i.e., poly(*N*-isopropylacrlyamide) aqueous solutions.

Introduction

The self-assembling in nanometer-order structures has recently been gathering much attention.[1−4] This is partially due to advancement of various types of living polymerization techniques, such as anionic, cationic, radical, metallocene polymerization, etc.[5] This advancement meets various types of demands for developing functional materials, such as drug delivery systems and artificial membranes. Block copolymers have long been recognized as typical systems capable of self-assembling, particularly in the last several decades.[6,7] The most characteristic feature of block copolymers lies in the presence of chemical junction connecting unlike polymer chains, which results in a nanometer-order phase separation, the so-called *microphase separation*. The microphase separation is governed by the molecular weights, the compositions, the interaction parameters of the constituent blocks, and the polymer concentrations if the block copolymer is in a solvent.[8] Two types of transitions, i.e., lattice ordering and order−disorder transition, were reported in a series of works on poly(styrene-*b*-butadiene) (PS−PB) in a selective solvent.[9−11] The former is a melting of macrolattice (or disordering of microphase separated structure) to micelles, and the other is dissolution of the micelles. These transitions were found to be thermoreversible and concentration-reversible, which are due to a strong selectivity of the solvent. The solvent used was *n*-tetradecane (C14), which is a selective solvent for polybutadiene (PB) and a nonsolvent for polystyrene (PS). By increasing temperature, PS becomes soluble to C14, which leads to lattice disordering followed by order−disorder transition. Recently, studies on ordering and/or morphological transitions of block copolymers in a selective solvent have been extensively carried out.[2,3,12,13] These transitions are ascribed to the temperature and/or concentration dependence of the van der Waals interaction between the polymer chain and solvent.

Scheme 1

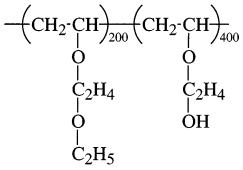

An amphiphilic block copolymer consisting of hydrophilic and hydrophobic block copolymer chains is expected to undergo micellization in water, where hydrophobic interaction plays a major role in controlling the morphology.[1,4] Aoshima et al. prepared a series of stimuli-responsive block copolymers with polyalcohol[14] and/or poly(vinyl ether) segments having oxyethylene units in the side group.[15−17] Because of a narrow molecular weight distribution, a sharp transition in turbidity as well as in viscosity with respect to temperature was observed. Among a variety of combinations, poly(2-ethoxyethyl vinyl ether-*b*-2-hydroxyethyl vinyl ether) (Scheme 1; hereafter we abbreviate it as poly(EOVE-*b*-HOVE)) aqueous solutions were chosen in this study because they undergo fluidity transition without accompanying serious turbidity. To elucidate the origin of this sharp transition, we carried out a microscopic investigation of poly(EOVE-*b*-HOVE) with small-angle neutron scattering (SANS). In a successive paper, we discuss the dynamics of poly(EOVE-*b*-HOVE) chains in water on the basis of data obtained with dynamic light scattering.

Experimental Section

1. Sample. The synthesis of poly(2-ethoxyethyl vinyl ether-*b*-2-hydroxyethyl vinyl ether), poly(EOVE-*b*-HOVE), involves (i) the preparation of precursor block copolymers by living cationic polymerization of 2-ethoxyethyl vinyl ether (EOVE)

* To whom correspondence should be addressed.
[†] The University of Tokyo.
[‡] Osaka University.

10.1021/ma020480+ CCC: $22.00
Published on Web 09/12/2002

and 2-(*tert*-butyldimethylsilyloxy)ethyl vinyl ether (BMSiVE) and (ii) the subsequent conversion of poly(BMSiVE) segments in the precursor block copolymers to poly(HOVE) segments by acid-promoted hydrolysis.[14] The monomer BMSiVE was prepared by the reaction of 1-(*tert*-butyldimethylsilyl)imidazole with 2-hydroxyethyl vinyl ether (Maruzen Petrochemical) in dimethylformamide at room temperature. The living cationic polymerization was carried out in the presence of ethyl acetate as an added base to stabilize the propagating species.[18] At first, EOVE was polymerized with $CH_3CH(OiBu)OCOCH_3/Et_{1.5}AlCl_{1.5}$ in toluene at 0 °C under a dry nitrogen atmosphere.[19] The second monomer, BMSiVE (neat), was then fed into the polymerization mixture. After a certain period, the polymerization was quenched with 0.1 wt % ammoniacal methanol. The quenched reaction mixture was diluted with dichloromethane and then washed with water to remove the initiator residues. The product polymer was recovered from the organic layer by evaporation of the solvents under reduced pressure and vacuum-dried overnight. Formation of the desired block copolymers was confirmed by size exclusion chromatography. The composition ratio determined by ^{1}H NMR spectroscopy (JEOL JNM-EX 270) was in agreement with the monomer feed ratio of EOVE and BMSiVE (1/2). Desilylation from poly(EOVE-*b*-BMSiVE) was carried out with the addition of 3.0 N aqueous HCl-EtOH to a purified polymer in THF at 0 °C, followed by stirring for 6 h at 0 °C. The mixtures were neutralized, filtered, and isolated by dialysis against Mill-Q water (18 MΩ cm) using a cellulose tube. The poly(EOVE-*b*-HOVE) was recovered by evaporation of water under reduced pressure and vacuum-dried overnight. Thus, poly(EOVE-*b*-HOVE) with $\bar{M}_n = 5.84 \times 10^4$, $\bar{M}_w/\bar{M}_n = 1.07$ was obtained, in which the degrees of polymerizations of EOVE and HOVE are 200 and 400, respectively.

2. Rheological Measurement. The dynamic viscoelastic measurement was carried out with a stress-controlled rheometer (Carri-Med CSL^2 100, TA-Instruments) with angular frequency of 6.283 rad/s (1 Hz). A cone plate with a diameter of 4 cm and an angle of 2° was employed. The temperature was controlled within 0.1 °C by a Peltier element.

3. Small-Angle Neutron Scattering (SANS). Since aqueous solutions of poly(EOVE-*b*-HOVE) lose fluidity above 20 °C, dry poly(EOVE-*b*-HOVE) was dissolved in cold deuterated water at ca. 0 °C and was kept in a refrigerator until use. The concentrations of poly(EOVE-*b*-HOVE) were 2, 5, 10, and 17 wt %. The SANS experiment was carried out at the SANS-U spectrometer, Institute for Solid State Physics, The University of Tokyo.[20] Cold neutrons from the JRR-3M research reactor of Japan Atomic Energy Research Institute, Tokai, Ibaraki, Japan, were monochromatized to a 7.0 Å beam with a neutron velocity selector. The wavelength distribution was 13%. The sample to detector distance was either 4 or 8 m. The temperature of the sample was regulated with a water circulating bath (NESLAB RTE-111 M). Samples in quartz cells of 1 or 4 mm thick were irradiated by the neutron beam for 30 or 60 min depending on the scattering power. The scattered intensity functions were corrected for transmission and air scattering and then circularly averaged. The subsequent absolute intensity calibration was carried out with the incoherent scattering from a Lupolen (polyethylene) secondary standard sample.[21]

4. Small-Angle X-ray Scattering (SAXS). The SAXS measurement was carried out on a 17 wt % poly(EOVE-*b*-HOVE) aqueous solution at room temperature (≈25 °C) with a SAXS instrument (Nano Viewer, Rigaku, Co. Ltd., Japan) equipped with an imaging plate. The X-ray beam was obtained by an X-ray generator (Rigaku Ultrax 18). The operating condition was 45 kV, at 60 mA, and the beam size was 0.3 × 0.3 mm^2. Monochromatization and intensification was attained with a confocal multilayered mirror optic (Confocal MaxFlux Optic (CMF)). A focused Cu Kα line (wavelength being 1.54 Å) was used for the SAXS measurement.

5. Differential Thermal Calorimetry. A high-sensitivity differential scanning calorimeter (DSC8230, Rigaku, Co. Ltd.) was used to study the endothermic enthalpy. About 26 mg of polymer sample was placed in a stainless pan (resistance to pressure at 50 atm, 3 × 5 o.d. mm for the vessel size) and then carefully sealed. Thermograms were obtained at rates of 1 °C/min in heating scans between −10 and +80 °C, with water in a stainless pan as a reference.

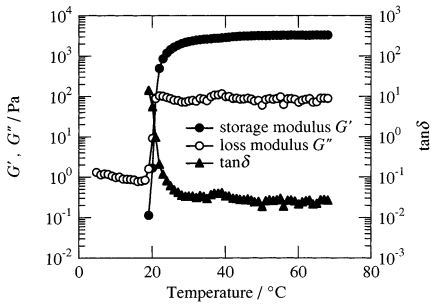

Figure 1. Temperature dependence of the storage (G') and loss moduli (G'') for poly(EOVE-*b*-HOVE) block copolymer aqueous solutions at $w = 20$ wt % (1 Hz).

Results and Discussion

1. Rheological Transition. Figure 1 shows a temperature scan of the storage (G') and loss moduli (G'') for a 20 wt % poly(EOVE-*b*-HOVE) aqueous solution. This shows a sharp transition in both G' and G'' around 20 °C. It is surprising that the change in G' is more than 4 orders of magnitude, and the temperature window of the transition is less than a degree centigrade. A similar transition was also observed for a 10 wt % poly(EOVE-*b*-HOVE) aqueous solution at almost the same temperature.

2. SANS Analysis. Figure 2 shows SANS intensity functions, $I(q)$, of poly(EOVE-*b*-HOVE) aqueous solutions at polymer concentrations of (a) $w = 2$, (b) 5, (c) 10, and (d) 17 wt %. Here, q is the momentum transfer. For all concentrations, $I(q)$ was a monotonically decreasing function at low temperatures, i.e., for $T \leq 20$ °C ($w = 2$ wt %), $T \leq 19$ °C ($w = 5$ wt %), $T \leq 17$ °C ($w = 10$ wt %), and $T \leq 16$ °C ($w = 17$ wt %). With increasing temperature, however, the forward scattering increased significantly and scattering peaks appeared. In addition, the peaks shifted toward higher q with increasing T. In the case of $w = 17$ wt %, a scattering peak appeared at 17 °C and $I(q)$ grew with further increasing temperature. It should be noted here that additional distinct peaks (denoted by arrows) appear at the lower q region for $T \geq 20$ °C. It is easily deduced that the $I(q)$s with these scattering maxima correspond to the form factor for spherical particles as will be discussed later. In the following, the SANS intensity functions are analyzed in the three regimes, i.e., (i) scattering from polymer solutions, (ii) micelle scattering, and (iii) macrolattice scattering.

2.1. Scattering Functions from Homogeneous Polymer Solutions. In the semidilute regime, the so-called correlation length ξ can be evaluated with the following Ornstein−Zernike equation:

$$I(q) = \frac{I(0)}{1 + \xi^2 q^2} \tag{1}$$

The values of the correlation length are about 60 Å for 2 wt %, 40 Å for 5 wt %, and 35 Å for 10 wt % irrespective of T. This indicates that ξ is a decreasing function of polymer concentration, w. The details will be reported elsewhere.

2.2. Form Factor and Curve Fitting with the Spherical-Particle Function. Here, we focus on the particle scattering from spherical domains. The form

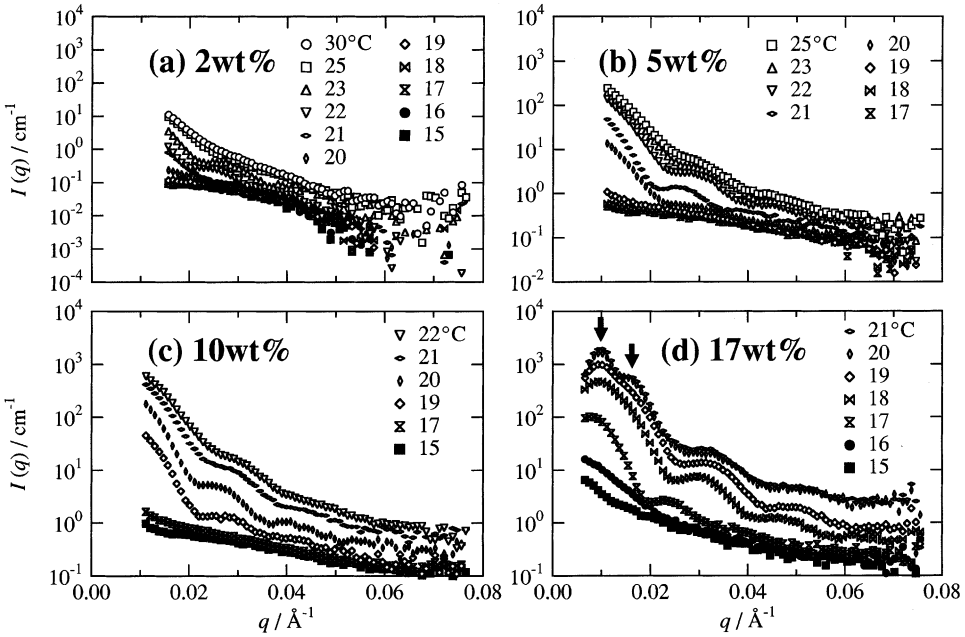

Figure 2. SANS scattering intensity curves of poly(EOVE-*b*-HOVE) aqueous solutions at (a) $w = 2.0$, (b) 5.0, (c) 10, and (d) 17 wt %. The arrows indicate the interference peaks due to formation of the macrolattice.

factor for a sphere, $\Phi^2(q)$, is given by

$$\Phi(qR) = \frac{3[\sin(qR) - qR\cos(qR)]}{(qR)^3} \equiv 3\sqrt{\frac{\pi}{2}}\frac{J_{3/2}(qR)}{(qR)^{3/2}} \tag{2}$$

where R is the radius of the sphere and $\Phi(x)$ is related to the Bessel function of the order of $^3/_2$, i.e., $J_{3/2}(x)$. The SANS intensity function for an assembly of dispersed spheres is given by

$$I(q) = nV^2\Delta\rho^2\Phi^2(qR) \tag{3}$$

where n is the number of spheres in the unit volume (e.g., cm^3), V is the volume of the sphere, and $\Delta\rho$ is the scattering-length density difference between the sphere and the matrix. The curve fitting of the observed intensity functions was carried out by considering several facts: (1) size distribution of spheres, (2) wavelength distribution of the incident neutron beam, and (3) the instrumental smearing due to a finite size of incident beam.

The size distribution, $W_R(R)$, was assumed to be a Gaussian function given by

$$W_R(R) \sim \exp\left[-\frac{(R - \langle R\rangle)^2}{2\sigma_R^{\,2}}\right] \tag{4}$$

where $\langle R\rangle$ is the average radius of the sphere. Hence eq 3 has to be rewritten to[22]

$$I_R(q) = \langle n\rangle\Delta\rho^2\frac{\int W(R)V^2(R)\Phi^2(qR)\,\mathrm{d}R}{\int W(R)\,\mathrm{d}R} \tag{5}$$

Here, $\langle n\rangle$ is the average number of spheres in a unit volume and is given by

$$\langle n\rangle = \frac{w}{d_p\langle V\rangle} = \frac{\int W(R)\,\mathrm{d}R}{\int W(R)V\,\mathrm{d}R} \tag{6}$$

The wavelength distribution of the SANS-U is estimated to be fwhm = 13% around $\langle\lambda\rangle = 7.0$ Å. Again, a Gaussian distribution was assumed for the wavelength distribution, $W_\lambda(\lambda)$, with

$$W_\lambda(\lambda) \sim \exp\left[-\frac{(\lambda - \langle\lambda\rangle)^2}{2\sigma_\lambda^{\,2}}\right],\ \sigma_\lambda = \mathrm{fwhm}/2\sqrt{2\ln 2} \tag{7}$$

and the corrected intensity, $I_{R+\lambda}(q)$, is given in the following form,

$$I_{R+\lambda}(q) = \frac{w}{d_p}\Delta\rho^2\frac{\int\int W_R(R)W_\lambda(\lambda)V^2(R)\Phi^2(qR)\,\mathrm{d}R\,\mathrm{d}\lambda}{\int\int W_R(R)W_\lambda(\lambda)V(R)\,\mathrm{d}R\,\mathrm{d}\lambda} \tag{8}$$

The effect of instrumental smearing was also taken into account by convoluting $I(q)$ with the incident beam profile function at the detector plane. The width of the incident beam was evaluated to be $\pm 1.35 \times 10^{-3}$ Å^{-1}. It was found that the dominant smearing effect is not due to the wavelength distribution but to the finite size of the incident beam. Figure 3 shows the results of curve fitting for $w = 17$ wt % at various temperatures. Except for $T = 20$ and 21 °C, the curve fitting seems to be satisfactory. The same analysis was applied to the other samples having different concentrations.

Figure 4 shows the concentration and temperature dependence of (a) the average radius of the core $\langle R\rangle$ and (b) its distribution $\Delta R/\langle R\rangle$. In the case of $w = 17$ wt %, $\langle R\rangle$ is a decreasing function of T, but $\langle R\rangle$ reaches a plateau value of ca. 180 Å. Although the values of $\langle R\rangle$ for $w \le 10$ wt % are somewhat scattered, the values are rather invariant with respect to both temperature for $T \ge 20$ °C and concentration, and are again 180−200 Å. Interestingly, the distribution $\Delta R/\langle R\rangle$ does not change with w or T, either. This indicates that the domain size and its distribution are not determined by the environmental variables, such as polymer concentration and temperature (as long as $T \ge 20$ °C), but by the molecular parameters, i.e., the length of poly(EOVE)

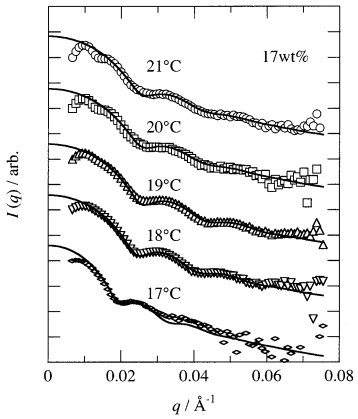

Figure 3. Results of curve fit of the SANS scattering intensity functions with eq 8 for poly(EOVE-*b*-HOVE) at $w = 17$ wt %.

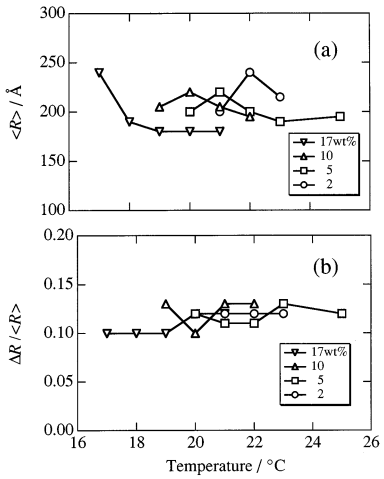

Figure 4. Temperature dependence of (a) the average radius of the poly(EOVE) domains, $\langle R \rangle$, and its distribution, $\Delta R/\langle R \rangle$, for poly(EOVE-*b*-HOVE) aqueous solutions at various concentrations.

and the block composition. It is noteworthy that this is quite different from the case of poly(styrene-*b*-butadiene) in a selective solvent, where the domain size is a strong function of polymer concentration and temperature due to partial solvation by the selective solvent.[10] However, in the case of poly(EOVE-*b*-HOVE), the hydrophobicity of poly(EOVE) is very strong above 20 °C, resulting in strong exclusion of water from the poly(EOVE) domain and formation of a spherical domain with a rather unique size. It should also be noted here that the domain size $\langle R \rangle$ is considerably larger than the radius of gyration of the polymer chain, $R_{g,z}$. This means that the poly(EOVE) chains in the spherical domains are not in the unperturbed but are highly stretched in the radial direction. The driving force of this chain stretching may be the lowering tendency of the total surface area by increasing the radius due to the strong hydrophobic interaction between poly(EOVE) and the solvent.

Figure 5a shows $I(0)$ vs T for poly(EOVE-*b*-HOVE) at various w's. $I(0)$ increases with T. This indicates that the micelle formation proceeds and the difference in the scattering length density increases with increasing T. Regarding w dependence, $I(0)$ can be normalized with concentration and the volume of the sphere, i.e., wV, since w is proportional to $\langle n \rangle$. Note that the number density of the spherical domains remains unchanged irrespective of temperature. By normalizing $I(0)$ with

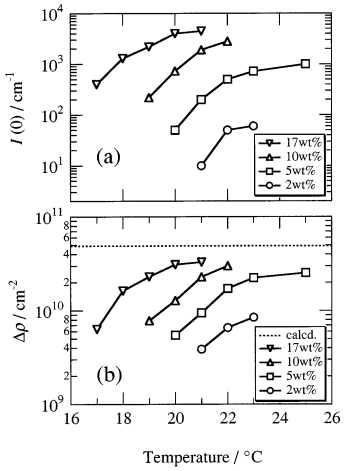

Figure 5. Temperature dependence of (a) the zero-q intensity, $I(q = 0)$, and (b) the scattering-length density, $\Delta\rho$. The dashed line indicates the calculated value for the perfect separation of poly(EOVE) from a mixture of poly(HOVE) and D_2O.

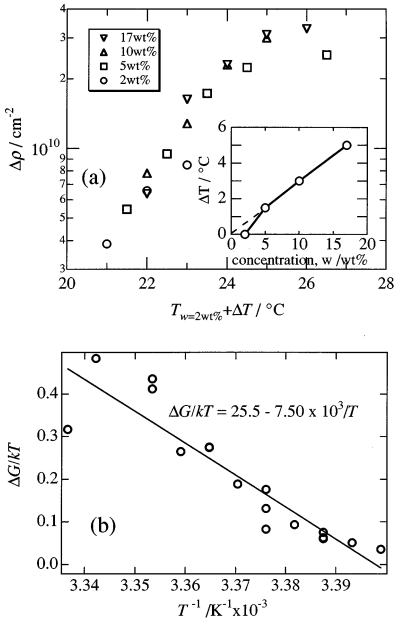

Figure 6. (a) Master curve of the scattering-length density, $\Delta\rho$, reduced by the polymer concentration and with a temperature-shift factor, ΔT. The inset shows the concentration dependence of the shift factor, ΔT. (b) Inverse temperature dependence of the energy of partition of to place EOVE segments in the core, ΔE.

wV, one obtains the variation of the contrast factor, i.e., the scattering-length density difference between the sphere and the matrix, $\Delta\rho$. In Figure 5b, $\Delta\rho$ is plotted as a function of T, which increases with T. The dashed line indicates the theoretical value for perfect separation of poly(EOVE) from a mixture of poly(HOVE) and D_2O ($\Delta\rho_0 = 4.9 \times 10^{10}$ cm^{-2}). Therefore, this plot shows that phase separation between micelle and matrix proceeds with increasing temperature. Figure 6 shows a master curve for the $\Delta\rho$ vs $T + \Delta T$. A horizontal shift was necessary to construct the master curve because the transition temperature is concentration dependent. The shift factor ΔT is shown in the inset of Figure 6a. This indicates that the interaction parameter between poly(EOVE) and water is a function of poly(EOVE) concentration as well as temperature and the transition temperature for micellization increases rather linearly with T. The dependence of poly(EOVE) concentration

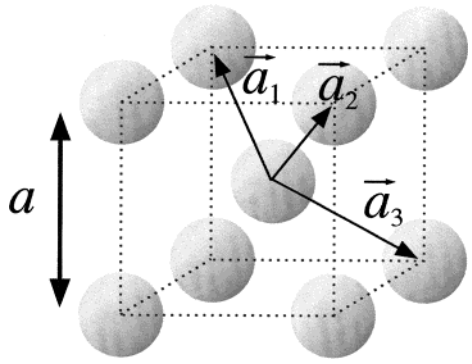

Figure 7. Unit cell of the body-centered cubic lattice and definition of the principal axes.

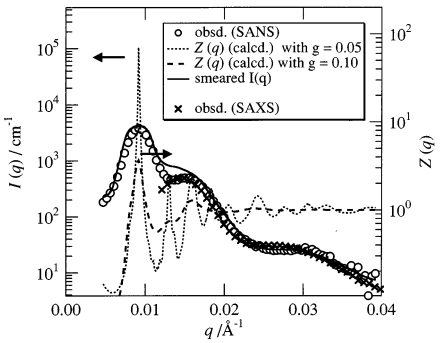

Figure 8. Result of curve fitting of the scattering intensity function for poly(EOVE-*b*-HOVE) (17 wt %, 26 °C) with Hosemann−Bagchi's paracrystal theory: observed SANS function (open circles), the lattice factor $Z(q)$ with $g = 0.05$ (dotted line) and $g = 0.10$ (dashed line), the smeared calculated-SANS function (solid line), and SAXS intensity.

is consistent with our preliminary results by using of homopolymers having a similar structure.[19]

The partition coefficient, i.e., the difference in the fraction of the EOVE segments in the core and the matrix, can be estimated via $\Delta\rho$, with the following equations[23]

$$\Delta\phi_{\mathrm{EOVE}} \equiv \left(\frac{\Delta\rho}{\Delta\rho_0}\right) = 1 - \exp\left(-\frac{\Delta G}{k_{\mathrm{B}}T}\right) \tag{9}$$

$$\frac{\Delta G}{k_{\mathrm{B}}T} = -\ln[1 - \Delta\phi_{\mathrm{EOVE}}] = \frac{\Delta H}{k_{\mathrm{B}}T} - \frac{\Delta S}{k_{\mathrm{B}}} \tag{10}$$

where k_{B} is the Boltzmann constant, ΔG (≥ 0) is the free energy difference to place an EOVE block chain in the domain and in the matrix, and ΔH and ΔS are the corresponding enthalpy and entropy, respectively. ΔG was evaluated by linear regression of eq 10

$$\Delta G/k_{\mathrm{B}}T = 25.5 - 7.50 \times 10^3/T, \quad T > 294\ \mathrm{K} \quad (\text{for } w = 2\ \text{wt \%}) \tag{11}$$

and

$$T = T_{w=2\mathrm{wt\%}} + \Delta T, \quad \Delta T = 0.29w(\text{wt \%}) \tag{12}$$

Figure 6b shows the plot of $\Delta G/k_{\mathrm{B}}T$ as a function of $1/T$. The enthalpy of partition, ΔH, is negative (≈ -15.0 kcal/mol) and is quite large, resulting in the strong temperature dependence of the phase behavior. A negative sign means that the system has a lower critical solution temperature (LCST), above which a phase separation takes place. The concentration dependence of ΔT is obtained from the inset of Figure 8a

$$\Delta T \approx 0.29w[\text{wt \%}], \quad 0 \leq w \leq 17\ \text{wt \%} \tag{13}$$

Hence, the partition coefficient is proportional to the polymer concentration in this regime.

2.3. Paracrystal Analysis. In this section, we discuss the scattering peaks appearing in poly(EOVE-*b*-HOVE) ($w = 17$ wt %). These peaks indicate formation of a macrolattice in the system. The paracrystal theory developed by Hosemann and Bagchi is suitable to describe the structure of the macrolattice.[24] The theory introduces the lattice factor, Z_k ($k = 1,2,$and 3), which is given by

$$Z_k(q) = \frac{1 - |F(q)|^2}{1 - 2|F(q)|\cos(\vec{a}_k\cdot\vec{q}) + |F(q)|^2} \tag{14}$$

where $F(q)$ is the factor relating the degree of distortion

$$|F(q)| = \exp\left[-\frac{1}{2}\frac{\Delta a^2}{a^2}\{(\vec{a}_1\cdot\vec{q})^2 + (\vec{a}_2\cdot\vec{q})^2 + (\vec{a}_3\cdot\vec{q})^2\}\right] \tag{15}$$

Here, a and Δa are the unit cell distance and its standard deviation, respectively. The ratio $g \equiv \Delta a/a$ is often called the Hosemann's g-factor, which determines the degree of paracrystallinity. In the case of a body-centered cubic (bcc) structure, the unit vectors of the principal axes a_1, a_2, and a_3 are defined as shown in Figure 7 and the scalar products are given by[25,26]

$$\begin{aligned}
\vec{a}_1\cdot\vec{q} &= \frac{1}{2}aq(\sin\theta\sin\phi + \sin\theta\sin\phi + \cos\theta)\\
\vec{a}_2\cdot\vec{q} &= \frac{1}{2}aq(-\sin\theta\sin\phi - \sin\theta\sin\phi + \cos\theta)\\
\vec{a}_3\cdot\vec{q} &= \frac{1}{2}aq(-\sin\theta\sin\phi + \sin\theta\sin\phi - \cos\theta)
\end{aligned} \tag{16}$$

Since the macrolattice is randomly oriented in the space, one needs an orientational average as given by

$$Z(q) = \frac{1}{4\pi}\int_0^{2\pi}\int_0^{\pi} Z_1(q,\theta,\phi)Z_2(q,\theta,\phi)Z_3(q,\theta,\phi)\sin\theta\,\mathrm{d}\theta\,\mathrm{d}\phi \tag{17}$$

Figure 8 shows the result of curve fitting with the paracrystal theory as well as the calculated lattice factor, $Z(q)$, for bcc lattice. The open circles denote the SANS data obtained with an extended camera length of 8 m for poly(EOVE-*b*-HOVE) at $w = 17$ wt % at 26 °C. The dot-and-dashed line denotes the lattice factors, $Z(q)$, with $a = 970$ Å for $g = 0.05$ and 0.1, respectively. The solid line denoted the curve-fitted result of the case with $g = 0.1$ by taking account of the smearing of the incident beam width and the wavelength distribution. Note that a curve fitting with the face-centered-cubic (fcc) lattice model did not work at all. To confirm this result, a supplemental study was carried out with small-angle X-ray scattering. The SAXS result is shown with crosses, which is in good agreement with the SANS result. Note that the incident beam width (fwhm) of the SAXS was $\pm 2.04 \times 10^{-3}$ Å^{-1}, which is about twice as large as that of the SANS. Therefore, the missing of the second peak of the bcc lattice is due not to the incident

beam smearing but to the ill-developed macrolattice of the poly(EOVE-*b*-HOVE), i.e., g (∼0.1) as was evaluated by curve fitting. According to McConnell et al.,[2] block copolymer systems in a selective solvent can take either fcc or bcc packing depending on the length scale of the corona chain length relative to the core dimension. When the corona length is larger than the core size, the system prefers a bcc packing, which is the case in this study.

2.4. Evaluation of the Volume Fraction of the Core and the Occupied Area on the Surface by a Single Chain. By knowing the Bragg spacing, L, and the radius of the sphere, $\langle R \rangle$, the volume fraction of domain can be estimated by the following relationship

$$L = a/\sqrt{2} = \sqrt{2/3}D_0, \quad \phi_j = \frac{4\pi}{3} j \left(\frac{\langle R \rangle}{a}\right)^3 \qquad (18)$$

where D_0 is the nearest neighbor distance, and j is the factor depending on the packing, i.e., $j = 1$ (sc), 2 (bcc), and 4 (fcc). Since we know the poly(EOVE-*b*-HOVE) forms a bcc lattice structure, we put $j = 2$, and by substituting $a_{bcc} = 970$ Å and $\langle R \rangle = 180$ Å on the basis of the data at $w = 17$ wt %, one gets $\phi_{bcc} = 0.054$. This value is in good accordance with the value ($\phi = 0.056$) evaluated by stoichiometry by assuming perfect exclusion of poly(EOVE) from others. On the other hand, substitution of $\langle R \rangle = 200$ Å at $w \leq 10$ wt % leads to an estimation of water content in the spherical domain. It is deduced that about 23% of the volume of the sphere is occupied by water. In this case, the scattering length density difference, $\Delta\rho$, can be reevaluated by using the value obtained here. The reevaluated value is 3.6×10^{10} cm^{-2}, which is also in good agreement with the observed one, 3.3×10^{10} cm^{-2} (Figure 5).

It is of interest to consider the area partitioned to a single chain on the surface of a core of a micelle. The number of block chains in a micelle, N, is estimated to

$$N = \frac{V}{Z_{EOVE} v_{EOVE}} = 633 \qquad (19)$$

where Z_{EOVE} and v_{EOVE} are the degree of polymerization and monomer volume of EOVE, respectively. Since the surface area of a corona is simply obtained by $S = 4\pi\langle R \rangle^2$, one obtains $(S/N)^{1/2}$ to be

$$(S/N)^{1/2} = 25 \text{ Å} \qquad (20)$$

Therefore, roughly speaking, an area of 25^2 Å^2 is partitioned to each block chain. Interestingly, this value is very close to the surface area occupied by a block polymer chain consisting of PS−PB block copolymer with polystyrene volume fraction being 0.26 in a selective solvent ($(S/N)^{1/2} \sim 24$ Å).[10] In the case of lamellar domain structure in a good solvent, a scaling relation is obtained[8]

$$(S/N)^{1/2} \sim \phi^{-1/3} \qquad (21)$$

Unlike the above case, the $(S/N)^{1/2}$ for poly(EOVE-*b*-HOVE) does not depend on the volume fraction of the polymer at least in the concentration range $2 \leq w \leq 17$ wt %. This may be due to a strong segregation at the surface of core.

3. Sharp Structural Transitions with Respect to Temperature. Figure 9 shows the phase diagram of poly(EOVE-*b*-HOVE) in aqueous solutions determined by SANS. It consists of three regimes, namely the regimes of (i) molecular mixture, (ii) micelles, and (iii) macrolattice. The solid lines dividing the individual regimes were drawn for the eye. As shown in this phase diagram, the disorder-to-order transition, i.e., from molecular mixture to micelles or macrolattice, is very sharp with respect to temperature and is on the order of subdegrees of centigrade. In addition, the phase-dividing line seems to be well represented by a monotonically decreasing function with concentration, indicating that the interaction parameter is a linear function of polymer concentration. This fact is in good agreement of the result of the analysis of $I(0)$ in which the contrast factor, $\Delta\rho$, is reduced to a master curve by employing a shift factor varying linearly with temperature (See Figure 6).

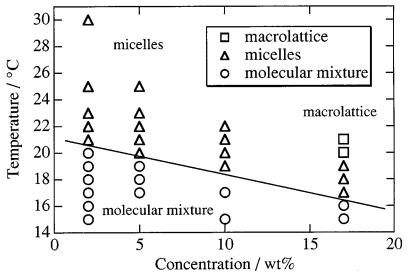

Figure 9. Phase diagram of poly(EOVE-*b*-HOVE) aqueous solutions, consisting of three phases: molecular mixture, micelles, macrolattice.

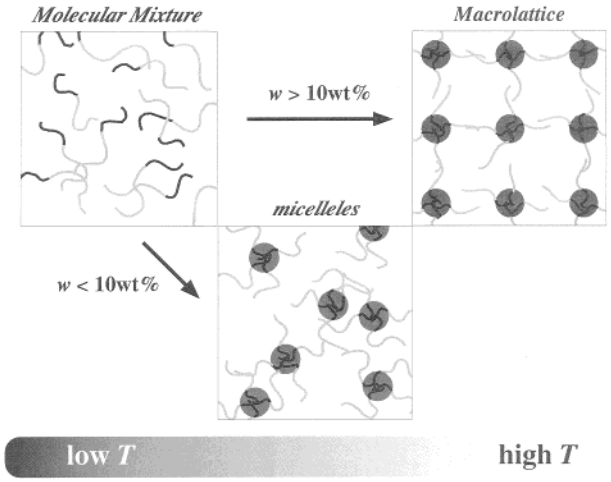

Figure 10. Schematic representation of showing two transitions from the molecular mixture (left) to the crystallike structure with macrolattice (right) by way of the micellar structure (middle).

Figure 10 shows the model of the assembly of poly(EOVE-*b*-HOVE) block copolymers in water. At low temperatures, the polymer chains are molecularly dispersed in the solvent. However, by increasing temperature, a micelle formation takes place and poly(EOVE) chains aggregate themselves in a core. The poly(HOVE) chains remain as brushes and play as emulsifier or surfactant. However, when the polymer concentration is high enough, morphological transition may take place directly from a molecular mixture to a macrolattice structure. This type of transition is commonly observed in various types of polyampholytes, such as poly(styrene-*b*-isoprene) (SI) block copolymer[2] and poly(ethylene oxide-*b*-propylene oxide) (PEO−PPO).[4] In the case of latter, a lyotropic morphological transition was observed. However, it should be emphasized that the

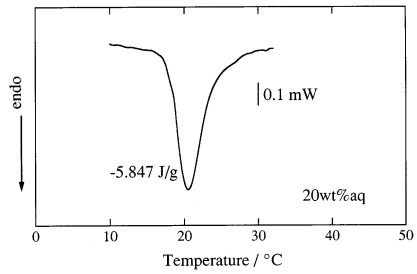

Figure 11. DSC thermogram of poly(EOVE-*b*-HOVE) aqueous solution with $w = 20$ wt %.

transition of poly(EOVE-*b*-HOVE) seems to be sharper than that of these systems.

4. Origin of the Sharp Transition. To elucidate the sharp disorder−order transition of poly(EOVE-*b*-HOVE) in aqueous solutions, a thermal analysis was carried out. Figure 11 shows the DSC thermogram of poly(EOVE-*b*-HOVE) aqueous solution with $w = 20$ wt %. As shown in the figure, a sharp endothermic peak was observed around $T = 20$ °C. The enthalpy for hydrophobic dissociation was observed to be −5.85 J for 27.3 mg for the solution, which is converted to $\Delta H = -2.05$ kcal/mol of EOVE. This value is about twice as large as that for poly(*N*-isopropylacrylamide) gel in water, i.e., $\Delta H_{NIPA} = -0.946$ kcal/mol of NIPA (3.95 kJ/mol of NIPA).[27] Note that the value of ΔH_{NIPA} itself is in good agreement with those by Otake et al. (−3.3 to −4.5 kJ/mol of NIPA).[28] It should be noted here that ΔH_{NIPA} for PNIPA gels is significantly smaller than that for PNIPA linear polymer solutions, e.g., 6.3 kJ/mol (Shild)[29] and −4.8 to −6.1 kJ/mol (Otake et al.),[28] which may be ascribed to a lowering of "the degree of hydrophobic hydration" in the gels by introducing the cross-linked structure. Shild[29] assigned this enthalpy change to hydrogen bond interaction. However, as discussed by Shibayama et al.,[27] it seems more reasonable to assign this endotherm as the dissociation enthalpy of the hydrophobic interaction.

The presence of this sharp endotherm around 20 °C clearly indicates that an iceberg melting takes place at this temperature. This causes a drastic change in the intermolecular interaction between EOVE segments and water molecules, resulting in a sharp morphological transition. This transition could be even sharper than a volume phase transition of NIPA gels because a larger endotherm is involved in the EOVE−water system. In the case of van der Waals interacting systems, the interaction parameter is a monotonic function of temperature and thermodynamic transition takes place as a result of the change of a delicate balance of enthalpic and entropic parts of free energy. On the other hand, the disorder−order transition of the poly(EOVE-*b*-HOVE) aqueous systems is governed by the enthalpy change due to melting of the iceberg structure, which is the first-order transition by the definition of thermodynamics. This is why the transition takes place with in a limited range of temperature irrespective of polymer concentration.

Conclusion

Nano-order structure formation of block copolymers (poly(EOVE-*b*-HOVE)) in aqueous systems has been studied by SANS as well as rheological and thermal analyses. The following facts were disclosed: (1) There exist disorder−order transitions, from a molecular mixture to micelles or a molecular mixture to macrolattice. The latter corresponds to a drastic change in macroscopic flow behavior, such as gelation. A phase diagram was constructed on the basis of the SANS results. (2) At low temperatures, the poly(EOVE-*b*-HOVE) block copolymer homogeneously dissolves in water, in which the correlation length ξ is evaluated to be 40 and 35 Å for 5 and 10 wt %, respectively, at the temperature range studied here. (3) In the micelle regime, the size of the core is 180−200 Å and is hardly dependent on either temperature or polymer concentration. (4) At higher temperatures and at higher polymer concentrations, a bcc macrolattice structure is formed with a unit cell of 970 Å and radius of 180 Å (for $w = 17$ wt %). (5) A master relationship is obtained for the scattering-length density difference, $\Delta\rho$, with a reasonable temperature shift factor, ΔT. This suggests that the scattered intensity is proportional to the polymer concentration. In other words, the micelle structures are rather identical to each other in the micelle phase, irrespective of polymer concentration. The temperature shift factor ΔT is a linear function of concentration, i.e., $\Delta T = 0.29w$, indicating that the polymer−solvent interaction parameter, χ, is also proportional to polymer concentration. (6) A significant amount of water could be associated in an EOVE core up to 23 wt % in the micelle phase. This water content agrees with the result of scattering-length density difference between the core and the matrix. (7) The surface area partitioned to a single block chain is about 25^2 Å^2, which is again in good agreement with another block copolymer systems consisting of PS−PB in a selective solvent. (8) The sharp structural transition was explained as a drastic endothermic change of miscibility between EOVE and water by iceberg melting with 2.05 kcal/mol of EOVE monomeric unit.

Acknowledgment. This work is partially supported by the Ministry of Education, Science, Sports and Culture, Japan (Grants-in-Aid 12450388 and 13031019 to M.S.). This work was performed with the approval of Neutron Scattering Program, Institute for Solid State Physics, The University of Tokyo (Proposal No. 01-1551). The authors are grateful to Rigaku, Co. Ltd., Tokyo, for their kindness in allowing us to use the SAXS instrument (Nano Viewer).

References and Notes

(1) Zhang, L.; Eisenberg, A. *Science* **1995**, *268*, 1728.
(2) McConnell, G. A.; Gast, A. P. *Macromolecules* **1997**, *30*, 435.
(3) McConnell, G. A.; Gast, A. P.; Huang, J. S.; Smith, S. D. *Phys. Rev. Lett.* **1993**, *71*, 2102.
(4) Alexandridis, P.; Ollson, U.; Lindman, B. *Langmuir* **1998**, *14*, 2627.
(5) Kobayashi, S. *Catalysis in Precision Polymerization*; Wiley & Sons: New York, 1997.
(6) Molau, G. E. in *Block Polymers*; Aggarwal, S. L., Ed.; Plenum Press: New York, 1970.
(7) Helfand, E.; Wasserman, Z. R. in *Developments in Block Copolymers*; Goodman, I., Ed.; Applied Science: New York, 1982.
(8) Shibayama, M.; Hashimoto, T.; Kawai, H. *Macromolecules* **1983**, *16*, 1093.
(9) Watanabe, H.; Kotaka, T.; Hashimoto, T.; Shibayama, M.; Kawai, H. *J. Rheol.* **1982**, *26*, 153.
(10) Shibayama, M.; Hashimoto, T.; Kawai, H. *Macromolecules* **1983**, *16*, 16.
(11) Hashimoto, T.; Shibayama, M.; Kawai, H.; Watanabe, H.; Kotaka, T. *Macromolecules* **1983**, *16*, 361.
(12) Huang, C. I.; Lodge, T. P. *Macromolecules* **1998**, *31*, 3556.
(13) Hamley, K. J.; Lodge, T. P.; Huang, C. I. *Macromolecules* **2000**, *33*, 5918.

(14) Aoshima, S.; Hashimoto, K. *J. Polym. Sci., Part A: Polym. Chem.* **2001**, *39*, 746.
(15) Aoshima, S.; Sugihara, S. *J. Polym. Sci., Part A: Polym. Chem.* **2000**, *38*, 3962.
(16) Sugihara, S.; Aoshima, S. *Koubunshi Ronbunshu* **2001**, *58*, 304.
(17) Sugihara, S.; Matsuzono, S.; Sakai, H.; Abe, M.; Aoshima, S. *J. Polym. Sci., Part A: Polym. Chem.* **2001**, *39*, 3190.
(18) Aoshima, S.; Higashimura, T. *Macromolecules* **1989**, *22*, 1009.
(19) Aoshima, S.; Oda, H.; Kobayashi, E. *J. Polym. Sci., Part A: Polym. Chem.* **1992**, *30*, 2407.
(20) Ito, Y.; Imai, M.; Takahashi, S. *Physica B* **1995**, *213&214*, 889.
(21) Schwahn, D.; Takeno, H.; Willner, L.; Hasegawa, H.; Jinnai, H.; Hashimoto, T.; Imai, M. *Phys. Rev. Lett.* **1994**, *73*, 3427.
(22) Hashimoto, H.; Fujimura, M.; Hashimoto, T.; Kawai, H. *Macromolecules* **1981**, *14*, 844.
(23) de Gennes, P. G. *Scaling Concepts in Polymer Physics*; Cornell University: Ithaca, NY, 1979.
(24) Hosemann, R.; Bagchi, S. N. *Direct Analysis of Diffraction by Matter*; North-Holland: Amsterdam, 1962.
(25) Matsuoka, H.; Tanaka, H.; Hashimoto, T.; Ise, N. *Phys. Rev. B* **1987**, *36*, 1754.
(26) Matsuoka, H.; Tanaka, H.; Iizuka, N.; Hashimoto, T.; Ise, N. *Phys. Rev. B* **1990**, *41*, 3854.
(27) Shibayama, M.; Mizutani, S.; Nomura, S. *Macromolecules* **1996**, *29*, 2019.
(28) Otake, K.; Inomata, H.; Konno, M.; Saito, S. *Macromolecules* **1990**, *23*, 283.
(29) Shild, H. G. *Prog. Polym. Sci.* **1992**, *17*, 163.

MA020480+